Ammonia emissions from a grazed field estimated by miniDOAS measurements and inverse dispersion modelling

Michael Bell[1], Christophe Flechard[1], Yannick Fauvel[1], Christoph Häni[2], Jörg Sintermann[3a], Markus Jocher[3], Harald Menzi[4], Arjan Hensen[5], Albrecht Neftel[3b]

[1]INRA, Agrocampus Ouest, UMR 1069 SAS, Rennes, France
[2]Bern University of Applied Sciences, School of Agricultural, Forest and Food Sciences, CH-3052 Zollikofen, Switzerland
[3]Agroscope - Institute for Sustainability Science, Zürich, Switzerland
[4]Federal Research Station Agroscope, Inst. For Livestock Sciences, 1725 Posieux, Switzerland
[5]Energy research Centre of the Netherlands (ECN), Petten, The Netherlands
[a]now at AWEL, Zürich, Switzerland
[b]now at Neftel research Expertise, C -3033 Wohlen b. Bern, Switzerland

Correspondence to: Michael Bell (michael.bell@inra.fr)

16   **Abstract**

17   Ammonia (NH_3) fluxes were estimated from a field being grazed by dairy cattle during spring, by applying a

18   backward-Lagrangian Stochastic model (bLS) model combined with horizontal concentration gradients

19   measured across the field. Continuous concentration measurements at field boundaries were made by open-path

20   miniDOAS (differential optical absorption spectroscopy) instruments, during the cattle's presence and for 6

21   subsequent days. The deposition of emitted NH_3 to 'clean' patches on the field was also simulated, allowing

22   both 'net' and 'gross' emission estimates, where the dry deposition velocity (v_d) was predicted by a canopy

23   resistance (R_c) model developed from local NH_3 flux and meteorological measurements. Estimated emissions

24   peaked during grazing and decreased after the cattle had left the field, while control on emissions was observed

25   from covariance with temperature, wind speed and humidity/wetness measurements made on the field, revealing

26   a diurnal emission profile. Large concentration differences were observed between downwind receptors, due to

27   spatially heterogeneous emission patterns. This was likely caused by uneven cattle distribution and a low

28   grazing density, where 'hotspots' of emissions would arise as the cattle grouped in certain areas, such as around

29   the water trough. The spatial complexity was accounted for by separating the model source area into sub-

30   sections, and optimising individual source area coefficients to measured concentrations. The background

31   concentration was the greatest source of uncertainty, and based on a sensitivity/uncertainty analysis the overall

32   uncertainty associated with derived emission factors from this study is at least 30-40%.

33   Emission factors can be expressed as 6 ± 2 g NH_3 cow^{-1} day^{-1}, or $9 \pm 3\%$ of excreted urine-N emitted as NH_3,

34   when deposition is not simulated, and 7 ± 2 g NH_3 cow^{-1} day^{-1}, or $10 \pm 3\%$ excreted urine-N emitted as NH_3

35   when deposition is included in the gross emission model. The results suggest that around $14 \pm 4\%$ of emitted

36   NH_3 was deposited to patches within the field that were not affected by urine or dung.

37   **1. Introduction**

38   Over 90% of anthropogenic ammonia (NH_3) emissions in Europe have agricultural sources (Erisman et al.,

39   2008; Reidy et al., 2008; Hertel et al., 2011), 70-90% of which have been estimated to be produced by livestock

40   (Pain et al., 1998; Hutchings et al., 2001). In addition to decreasing nitrogen efficiency for farming systems, the

41   volatilisation of NH_3 from agricultural areas is a principal factor in the formation of fine fraction secondary

42   aerosols due to its reactions with nitric and sulphuric acids in the atmosphere, and upon deposition is linked to

43   acidification and eutrophication of natural ecosystems (Sutton et al., 2011). Following the application of urine

44   and dung to the soil surface by grazing livestock, urea is microbially converted to NH_3 which is volatilised at

45   rates which vary extensively depending on soil and canopy layer properties, weather, and culture conditions

46   (Laubach et al., 2013a). It has been estimated that 75-90% of the N ingested by a grazing cow is metabolised

47   inefficiently and returned by excreta to the grazing paddocks, of which over 70% is returned as urine

48   (Whitehead, 1995; Zaman et al., 2009). NH_3 emissions have been measured from cattle urine patches at the ratio

49   of 7-25.7% of excreted urine nitrogen (N) for grazed pastures (Jarvis et al., 1989; Ryden et al., 1987; Laubach et

50   al., 2012; 2013a), and measurements from sheep urine patches in summer-winter experiments have suggested

51   emissions which represent 12.2–22.2% of excreted urine-N (Sherlock and Goh, 1984).

52   Methods for estimating emissions from grazed pastures include micrometeorological methods, where profiles of

53   concentration and wind speed are measured at one or more points downwind from the source, allowing fluxes to

54   be calculated using the theory of turbulent transport in the atmospheric surface layer (Laubach et al., 2012).

55   Dynamic chambers or movable wind tunnels may be used to estimate emissions from simulated grazing in the

56   laboratory or the field (Sommer et al., 2001). However enclosure measurements may not always be

57   representative of emissions at the field scale (Genermont and Cellier, 1997; Sintermann et al., 2012). The

58   inverse dispersion method concerns the inferring of the atmospheric emission rate (Q) of localised gas sources

59   from the excess concentration (ΔC) they cause above background, by modelling the $\Delta C/Q$ relationship for a

60   given source-receptor configuration and meteorological state (Flesch et al., 2004; Flesch et al., 2014).

61   The local dry deposition of NH_3 within the grazed field is an important consideration to make, as in contrast to

62   other pollutants a significant proportion may be deposited locally (e.g. Loubet et al., 2009). The proportion of

63   deposited NH_3 is sensitive to multiple parameters, including the source height, wind speed, atmospheric

64   stability, land cover type and the numerous specific surface parameters therein (e.g. Sutton et al. 1993). This

65   leads to modelling results that vary widely, with local recapture ranging from 2% to 60% within 2km from the

66   source (Loubet et al., 2006, Asman et al., 1998). Accordingly, the modelling of NH_3 deposition can be a

67   challenging undertaking, with models ranging from simple steady-state canopy resistance models to dynamic,

68   bi-directional, multi-layer and multi-process chemical species schemes (Flechard et al., 2013). Local-scale

69   deposition models may ignore the wet deposition process, as dry deposition is most likely the dominant

70   deposition mechanism near sources (Loubet et al., 2009).

71   In this study, a bLS (backward Lagrangian Stochastic) dispersion model with a coupled dry deposition scheme

72   has been applied to estimate the NH_3 emissions from a field being grazed by dairy cows, using the horizontal

73   concentration gradients measured across the field by three open-path miniDOAS instruments (Sintermann et al.,

74   2016; Volten et al., 2012). The open-path measurement system is to considerable benefit, as most techniques to

75   measure atmospheric NH_3 are sampling techniques and therefore involve inlet contact with the highly adhesive

76   NH_3, which may slow response times and lead to interaction with water molecules and interference by

77   ammonium aerosols dissociating on tubes or filters (e.g. von Bobrutzki et al., 2010). The miniDOAS system is a

78   comparatively interference-free measurement technique, since it utilises the wavelength-dependent UV-light

79   absorption of NH_3 over an open light path. The system also has capacity for long-term fast response continuous

80   measurements, and a broad measurement path which makes the miniDOAS a well-suited concentration receptor

81   for monitoring the fluctuations in NH_3 concentrations across field boundaries.

82   The objectives of our study were: (1) to evaluate the NH_3 emissions from cattle grazing using the bLS

83   dispersion technique and contribute towards an emission factor, as there is a limited number of existing

84   measurements, (2) to simulate the degree of re-deposition that occurs within the field, and (3) evaluate the

85   application of the bLS technique and the miniDOAS measurement system to derive NH_3 fluxes from

86   agricultural diffuse sources such as grazing. It was assumed that emission estimates would be insensitive to

87   irregular cattle distribution and excretion patterns. The measurement of concentration gradients across grazed

88   fields is challenging, as downwind concentration levels may not rise far above background as is the case with

89   stronger sources, such as applied slurry. Therefore, this is an exercise which requires precise and continuous

90   measurements from two or more sensors to evaluate (ΔC). However, the method is also non-intrusive and is not

91   labour intensive, and can provide continuous emission estimates over long or short time periods if the conditions

92   and experimental design are in agreement.

2. Methods

2.1 Site description and experimental design

The experiments were conducted from 18-29 May 2015, on a rectangular grazing pasture of about two hectares at the INRA-Méjusseaume dairy research experimental farm in NW France (48°07'01.3"N 1°47'50.5"W). The site was flat and benefited from a lack of wind-disturbing elements within 100m of the field boundaries (e.g. trees, buildings or other protruding elements). The cattle were not given additional feed to supplement grazing (mixed grass sward rich in *Lolium perenne*). The field had been previously grazed one month prior (16-27 May 2015) to the beginning of the experiment, and mineral fertiliser had been applied on 31/03. During measurement Period 1, 25 cows were grazing within the southwestern section of the field (Area D, Figure 1) from 08:00 18/05 - 15:00 20/05 UTC (28 hours grazing), with three sets of miniDOAS open-path sensors and placed along the northern, western and eastern boundaries. The miniDOAS sensors were placed to optimise the measurement of (ΔC) across the field after reviewing wind directions forecast for the week ahead. The miniDOAS sensors have been given the names S1, S2 and S3, where the S2 sensor was placed upwind of the grazed field while the S1 and S3 sensors were placed at downwind locations. During Period 2, the whole field (Areas A, B, C, D) was opened for 44 grazing cattle, with the cattle present on the field from 10:00 20/05 – 05:00 23/05 (60 hours grazing), while the miniDOAS sensors were left in place to measure residual emissions from 23-29/05. The cattle were removed from the field for milking during both periods for roughly one hour twice per day. As the field area during Period 2 was much larger, the S2 and S3 miniDOAS sensors were moved to the north-western and south-eastern field boundaries respectively, leaving the three miniDOAS paths in-line with a NW-SE transect of the field (Figure 1). The grazing densities during Periods 1 and 2 were 44 and 22 cattle ha^{-1}, respectively.

2.2 Ammonia measurements

The DOAS technique is based upon the wavelength dependent absorption of light over a specified light path. The miniDOAS instruments offer greater portability and a lower cost relative to prior DOAS instruments (Volten et al., 2012). The broadband and narrowband extinction of UV-light (=absorption + scattering) is measured across the light path, and the concentration of different trace gases is determined by their respective absorption spectra (details in Sintermann et al., 2016). In the wavelength range used by the miniDOAS (204 – 230nm), narrowband-absorption is seen by NH_3, sulphur dioxide (SO_2), and nitrogen oxide (NO), while other absorbers with broader absorption features are eliminated by high-pass-filtering. The systems were calibrated prior to the field experiment using a flow-cell in the miniDOAS light path with a high-concentration NH_3 gas standard; in addition, the cell's outlet-flow was checked by wet chemical impinger samples (two in a row) and photometric NH_3 determination. Reference spectra (I_{ref}, see Sintermann et al., 2016) were determined for each instrument at the field site one week prior to the grazing experiment, where the three miniDOAS systems were configured to measure in parallel (measuring concentrations across the same open-path). In order to provide the absolute concentration reference (c_{ref}, see Sintermann et al., 2016) for the miniDOAS, a transect of three sets of ALPHA passive sampler triplicates (Tang et al., 2001) were placed along the path length, giving a time-integrated c_{ref} measurement. The miniDOAS inter-comparison showed close agreement in the concentration levels between the three systems, where the coefficient of variation was 3.4% (unpublished data). The random

131 uncertainty of the miniDOAS measurements was determined to be 1.4% of the concentration levels, however
132 not lower than 0.2 µg m^{-2} s^{-1} (Sintermann et al., 2016). Since the initial miniDOAS publication (Sintermann et
133 al., 2016) the calibration procedure has been revised to correct a gas standard error in the conversion from ppm
134 to µg m^{-3}. The corrected measurements presented in this study are a factor of 1.16 higher relative to the NH$_3$
135 concentrations presented by Sintermann et al., (2016).

136 To measure horizontal concentration gradients across the field, three miniDOAS instruments were placed
137 strategically (based on the forecasted wind direction) at field boundaries at heights 1.4m above the ground, on
138 stands drilled into the ground for stability. Retro-reflectors were set 37m away from each light source at the
139 same height. A sensor placed upwind of the field would measure the background concentration (C_b), which can
140 be subtracted from the downwind concentration measurements (C) to determine the horizontal concentration
141 gradient or excess in concentration caused by emissions (ΔC). The miniDOAS concentration measurements
142 were recorded at 1-minute averaging intervals, and later averaged to 30 minute intervals for analysis.

143 **2.3 Micrometeorological measurements**

144 A three-dimensional ultrasonic anemometer (Gill Windmaster, Gill Instruments Limited, Lymington, UK) was
145 mounted on an instrument tower at 1.5m height above the ground within a fenced-off section in the centre of the
146 field. The sonic anemometer measured the three orthogonal wind components (u, v, w, m s^{-1}) at a frequency of
147 20 Hz, along with a fast temperature measurement. Later the eddy covariance measurements were processed
148 over 30 minute averages, and the friction velocity ($u*$, m s^{-1}), surface roughness (z_0, cm), Monin-Obukhov
149 length (L, m), standard deviations of the rotated wind components ($\sigma_u, \sigma_v, \sigma_w$), and resultant horizontal wind
150 speed (u, m s^{-1}) and wind direction (wd) were computed. Correction factors were applied to fix a 'bug' implicit
151 within the Gill Windmaster instrument, as recommended by the manufacturer (Gill Instruments, 2016). The
152 applied correction was a multiplication factor of 1.166 applied to positive vertical w wind axis measurements,
153 and a factor of 1.289 applied to negative w wind axis measurements.

154 Mounted on the instrument tower at 2m height was a HMP45C sensor (Campbell Scientific, Loughborough,
155 UK) which provided temperature (T, ᵒC) and relative humidity (RH, %) measurements. Leaf wetness (LW, %
156 time wet) at canopy level was measured by a specialised conductivity sensor (Campbell Scientific,
157 Loughborough, UK) placed 10 cm above the ground.

158 **2.4 Dispersion modelling**

159 The bLS type dispersion model is frequently applied for the computation of the inverse dispersion method
160 (Flesch et al., 2004). Driven by measurements of the prevailing wind conditions, and with knowledge of the rise
161 in concentration above background (ΔC) caused by an emitting source, the model can be applied to estimate the
162 emission rate that best fits the measured concentration data. The measured wind statistics ($\sigma_u, \sigma_v, \sigma_w$),
163 atmospheric frictional velocity ($u*$), wind direction (wd) and surface roughness (z_0) describe the windflow
164 characteristics, surface drag and buoyancy which enables the dispersion model to relate the downwind
165 concentration fields to emissions from the source area. Within the horizontally homogenous surface layer
166 (height z <100m, but above canopy level), the wind and turbulence measurements should be representative of
167 the atmosphere over the entire site, thus the sonic anemometer location is not critical. A condition of the bLS

168 method states that the terrain should be tolerably homogenous (Flesch et al., 2004), this criterion was met by the

169 study site which consisted entirely of short grass (10-20cm canopy height).

170 During bLS simulation the trajectories of thousands of fluid particles are calculated backwards in time from a

171 reference point (concentration receptor) under the prevailing wind conditions. The locations where the

172 trajectories intersect the ground ("touchdowns") and proportion of these which fall within the source area

173 (N_{source}) are used to calculate ($\Delta C/Q$), along with the associated vertical velocity (w_0) of each touchdown (for

174 details see Flesch et al., 1995; 2004).

175 The bLS-R model (Häni, 2016), is an inverse dispersion model that is based upon the backward Lagrangian

176 stochastic dispersion theory described by Flesch et al., (1995; 2004); however bLS-R has an additional function

177 which computes the effect of dry deposition on gas concentrations. The bLS-R package provides functions to set

178 up and execute the model within the R statistical software (R Core Team, 2015). Driven by the wind and

179 turbulence inputs, for each time interval the model calculates a dispersion coefficient D (s m^{-1}) specific to the

180 source-receptor geometry. The emission flux (Q, µg m^{-2} s^{-1}) may then be calculated from the measured rise in

181 concentration above background (ΔC) (Eq. 1).

$$Q = (\Delta C) * D^{-1} \tag{1}$$

183 where D is retrieved by the model from the number of source area interactions (N_{source}) and the thousands of

184 trajectories (N) released backwards in time from the receptor locations (Eq. 2), and the vertical "touchdown"

185 velocities" at impact (w_0) (for details see Flesch et al., 2004).

$$D = \frac{1}{N}\sum_{N_{source}} \left|\frac{2}{w_0}\right| \tag{2}$$

187 The following input data were applied in the bLS-R model as 30 minute averages: wind direction, frictional

188 velocity ($u*$) the standard deviations of the rotated wind vector components ($\sigma_u, \sigma_v, \sigma_w$), and surface roughness

189 (z_o). The spatial dimensions of the grazed field source area and the miniDOAS receptors were also specified.

190 Independent concentration measurements and emission estimates were derived using the two downwind

191 miniDOAS receptors (S1 and S3), which are compared throughout the paper, e.g. CS1, CS3 and QS1, QS3. All

192 concentrations and fluxes are expressed in units of NH$_3$, e.g. µg NH$_3$ m^{-3} and µg NH$_3$ m^{-2} s^{-1}.

193 **2.5 Data filtering**

194 The miniDOAS NH$_3$ measurements were filtered to remove periods of high uncertainty, indicated by the

195 standard error (SE) of the measurements. This filter only affected the S1 miniDOAS sensor, which was not

196 fitted with an automatic alignment system to correct minor shifts in the light path between lamp and reflector.

197 After applying this filter 92 out of 430 half hourly measurements were removed from the Period 2 S1

198 measurements (Period 1 measurements were unaffected).

199 Previous studies (Flesch et al., 2004; Harper et al., 2011) have applied $u*$ and Monin-Obukhov length (L)

200 filtering to remove emission estimates that do not meet given criteria ($u* > 0.15$ ms^{-1} and $L > 10$m). These

201 criteria were established on the basis of an observed reduction in the accuracy of model predictions as $u*$ and L

202 decrease (e.g., Flesch et al., 2004; Gao et al., 2009). However, filtering out periods with low wind speeds and

203 unstable stratification can be detrimental to emission estimates, often creating a bias to characterise certain

204 sources under specific daytime or night-time conditions, whilst ignoring potentially valuable data that do not

205 meet the criteria. This is a major limitation as we calculate average emissions from grazing cattle, where strong

206 diurnal cycling is expected to occur (e.g. Laubach et al., 2013a). Flesch et al., (2014) developed alternate criteria

207 for bLS data filtering, finding that (for their particular experiment) the $u*$ threshold could be reduced to 0.05 m

208 s^{-1}, and after finding no improvement after imposing a stability (L) filter, introduced a supplementary vertical

209 temperature gradient filter.

210 A filtering procedure was developed after assessing the standard error (SE) of emission estimates ($\sigma_{Q/Q}$), which

211 describes period-to-period fidelity and identifies "spiking" in model predictions caused by unsuitable input

212 conditions, which do not confirm to an underlying assumption of a horizontally homogenous surface layer

213 (Flesch et al., 2014). It was found that a $u*$ threshold of 0.1 m s^{-1} was sufficient to remove the significant

214 outliers, while retaining acceptable data coverage, although this filter was at times limiting for nocturnal (low

215 wind) periods. A wind direction filter was applied to remove periods where miniDOAS sensors S1 and S3 were

216 not downwind of the field area. This filter only affected sensor S3 during Period 2, where estimates were

217 ignored if $wd > 30$ & $wd < 270$.

218 **2.6 Modelling of dry deposition within the source area**

219 Downwind from a source of NH$_3$, local recapture will remove a certain fraction of emitted NH$_3$ from the air.

220 Therefore, the measured rise in concentration above background (ΔC) is a function of the source emission rate,

221 atmospheric dispersion, and the fraction that has been deposited. Within a field being grazed by dairy cattle,

222 emissions of NH$_3$ are expected from urine and dung patches, while deposition will occur to clean surfaces

223 within and beyond the field. As we apply the bLS method to estimate emissions from the measured

224 concentration gradient across the field (ΔC), we calculate the "net" flux constituting emissions from the field

225 minus the fraction that has been deposited. However, if dry deposition is simulated in the dispersion model the

226 lost fraction of emissions due to deposition can be quantified, providing an estimate for the "gross" emissions

227 from excretions during grazing.

228 The bLS-R model has a post-processing routine to simulate the effect of the dry deposition of NH$_3$ on flux

229 predictions. The exchange or deposition velocity (v_d, cm s^{-1}) is based upon a uni-directional resistance model

230 approach, defined as the inverse of a sum of a series of resistances to deposition (Eq. 3, left side) (Wesley and

231 Hicks, 2000).

$$v_d = \frac{1}{R_a + R_b + R_c} = \frac{-F}{C} \tag{3}$$

233 where R_a is the aerodynamic resistance to transfer through the turbulent surface layer for a certain reference

234 height, R_b is the boundary layer resistance associated with the viscous quasi-laminar sublayer adjacent to the

235 deposited surface, and R_c is the canopy resistance representing the combined surface resistance accounting for

236 stomatal and non-stomatal pathways to deposition (Flechard et al., 2013). It should be noted that R_a is implicit

237 within the bLS-R calculations and does not need to be input to the model as a variable.

238 The uni-directional resistance model treatment is based upon strongly simplified assumptions regarding the

239 near-ground NH$_3$ concentrations and respective NH$_3$ deposition flux, since the exchange of NH$_3$ to ecosystems

240 is bi-directional, involving many complex processes (Kruit et al., 2010; Fowler et al., 2009; Flechard et al.,

241 2013).

242 The resistances to deposition R_a and R_b can be calculated using ultrasonic anemometer measurements and well-

243 established models (Asman, 1998), while R_c is a composite term representing numerous physical barriers to

244   deposition at the surface. To obtain local, field-scale estimates of R_c, two COTAG systems (conditional time-

245   averaged gradient systems, Famulari et al., 2010) were operated at the centre of the grazed field for 1.5 years,

246   allowing R_c to be estimated from calculations of R_a and R_b and time-integrated measurements of NH_3

247   concentration (C), flux ($-F$) and v_d (Eq. 3). The COTAG measurements were filtered to remove grazing

248   periods and periods up to two weeks after grazing had ended, to ensure 'clean' background conditions. Clear

249   correlation was then observed between the time-integrated R_c estimates with the variables T (°C) and RH(%),

250   thus a double exponential equation was parameterised as follows to fit the data (Eq. 4, Figure 2), with similar

251   form to Flechard et al., (2010):

252    $$R_c = R_{c,min} \times exp^{\alpha \times (100-RH)} \times exp^{\beta \times Abs(T)} \qquad (4)$$

253   A curve fitting procedure provided estimates of the parameters α, β and $R_{c,min}$ as 0.013 and 0.015 °C^{-1} and 10 s

254   m^{-1}, respectively.

255   The deposition component of bLS-R operates on the assumption that the whole grazed field is acting as a

256   homogenous surface for deposition, however in reality urine and dung patches on the field are obviously

257   hotspots of emissions, and not NH_3 sinks. The ratio of 'clean canopy' where deposition may occur to 'soiled

258   canopy' is not known, thus it is difficult to provide a true emission estimate including the effect of deposition.

259   We can expect that the emission estimate without deposition (Q) represents a 'net' emission rate from the field,

260   while if we assume that the whole field behaves as homogenous sink, the emission rate including deposition will

261   represent an upper limit of the gross emission estimate. The actual emission rate for a soiled field can be

262   expected to fall somewhere in between the net and upper gross estimates.

263   A means of addressing this issue with the heterogeneous canopy surface may be found in reviewing the R_c

264   timeseries derived from the time-integrated COTAG concentration and flux measurements on the field, as v_d

265   acts on the local vertical concentration gradient between surface and reference height, i.e. the flux is

266   concentration-gradient driven. At certain periods over the course of the year cattle were brought onto the field

267   for grazing, and shortly after the grazing periods had ended the NH_3 flux would return back to the negative

268   (deposition), and therefore R_c could be calculated. Averaging all the COTAG R_c calculations within one month

269   following each grazing period gives an R_c value of 260 s m^{-1}, and comparing this value with the average R_c

270   where there had been no grazing on the field for at least one month (130 s m^{-1}). However, there was

271   considerable scatter in the data, with standard deviations of 200 s m^{-1} and 40 sm^{-1} for the post-grazing and

272   "clean" periods respectively. Fertilisation of the field surface through grazing appears to have caused an

273   increase in R_c of 130 s m^{-1}. This measured increase caused by excreted N to the field surface has been applied

274   as an offset to the modelled R_c estimated by Eq. 4, and has been input to bLS-R. The bLS emission estimates

275   without including deposition are referred to as Q, while the estimates including deposition and the R_c offset are

276   referred to as Q_{dep}. Emission estimates including deposition but without the R_c offset are referred to as

277   Q_{depmax}.

278   **2.7 N excretion model**

279   To contribute towards an emission factor for cattle grazing and to compare with literature values, it was

280   necessary to express the emission estimates as a fraction of excreted N or urine-N. A nitrogen excretion model

281   based on the Swiss feeding recommendations for dairy cows (Menzi et al., 2015; Muenger personal

communication) was applied to quantify the total N and urine-N excreted to the field during both grazing periods, from the following set of inputs: (1) milk yield, (2) animal numbers, average weight and date after calving, (3) the net energy for lactation (NEL) and crude protein (CP) content of the grass, (4) the number of animals grazed and the duration of grazing on the experimental plot. The excretions per day were calculated as consumption minus retention in milk and animal growth. The share of N excreted in faeces and urine was calculated using regressions of fecal N digestibility derived from N balance studies (Bracher et al., 2011; 2012).

3. Results

3.1 Period 1 (18-20/05): grazing on SW paddock only

3.1.1 Concentration measurements

The wind direction during Period 1 was consistently W-WSW (Figure 3). Therefore, DOAS S2 was located upwind of the grazed SW paddock while S1 and S3 were situated downwind to the eastern and northeastern boundaries of the field respectively. Concentrations across the S2 path length would be expected to be low and near background, except during periods of very low wind speed, while any rise in concentration measured by S1 and S3 above S2 would show the influence of emissions from the field.

The upwind S2 concentration measurements reveal background concentrations of 2-3 µg m^{-3} during times of steady W/SW winds, increasing slightly when wind speed was low. Concentration polar plots (Figure 3) show the average concentrations measured as a function of wind speed and direction, where the influence of emissions from the grazed field is illustrated by the increase in measured concentrations at downwind receptors S1 and S3 relative to S2 (C_b).

Power failure led to a partial loss of measurements from miniDOAS S2, which are required to specify C_b for estimating emissions through bLS modelling. A significant linear regression was found between the measured background S2 concentration and wind speed (u, m s^{-1}), temperature (T, °C) and relative humidity (RH, %):

$$C_b = 4.26 - 0.59u + 0.06T - 0.017RH, \text{r}^2 = 0.5 \tag{5}$$

The wind direction remained consistent after the S2 power failed on 19/05, therefore the empirical relationship (Eq. 5) was found to be suitable and was applied to estimate and extend S2 concentrations, as a proxy for C_b. The predicted S2 concentrations follow the measured S2 concentrations closely until the point of data loss on 19/05 (Figure 4, top panel). This lends confidence to the rest of the C_b predictions used to fill the gap in the measurements, even though there is increased uncertainty associated with the last 15 hours of emission estimates calculated from the predicted C_b, relative to periods where C_b was measured by the S2 sensor.

3.1.2 Field-scale emissions estimates

Overall there is very good agreement between the emission calculations from both downwind concentration datasets. The average emission rate calculated by bLS-R for the S3 measurements (QS3) is 0.29 µg m^{-2} s^{-1}, while the QS1 average is 0.27 µg m^{-2} s^{-1}. The modelled emission of NH$_3$ is low (generally below 0.2 µg m^{-2} s^{-1}) during the first 24 hours, as the measured concentration gradient across the field was less than 1 µg m^{-3}. As the cattle were introduced to the field on the first morning (18/05) it likely took some time for NH$_3$ to 'build up' from hydrolysis of excreted urea before significant emissions occurred. Downwind concentrations (CS1 and

318 CS3) peaked during the next day (19/05), with peak emissions occurring at midday when there was a 5-6 µg m^{-3}

319 horizontal concentration gradient (ΔC) measured between the upwind and downwind receptors. The peak

320 emission rate at this time was around 1.1 µg m^{-2} s^{-1} for both downwind receptors. A decrease in the measured

321 downwind concentrations occurred at 15:00, and an associated decrease in emissions is logically estimated for

322 this time period. The decline in emissions follows 4.4 mm of rain during the day of 19/08, where the rainfall

323 intensity peaked shortly after midday. In addition, the cattle were removed from the field at 15:00; therefore the

324 suspension of excretions to the field and the wet conditions are most likely the dominant factors driving the

325 declining emissions. The LW sensor indicated that the canopy was wet (conductivity reading above baseline) for

326 84% of Period 1 (Table 2).

327 Coinciding with the daytime peak in emissions and downwind concentrations were peaks in T and u, while RH

328 reached a minimum (Figure 4). During the night emissions decreased to near 0, where RH reaches a maximum

329 and T and u reach a minimum. The average Q_{dep} gross emission estimates are greater than the Q net emission

330 estimates by 13-16%.

331 **3.2 Period 2 (20-29/05): grazing on whole field**

332 **3.2.1 Concentration measurements**

333 Concentration measurements during Period 2 (20-29/05) revealed considerable differences between downwind

334 receptors, where the average CS1 at the center of the field was much greater than the average CS3 at the SE

335 corner (Figure 5), with period averages of 5.6 µg m^{-3} and 3.9 µg m^{-3}, respectively. This may be partially

336 explained by the location of the receptors relative to the grazed field under the prevailing wind conditions.

337 Sensor S1 was located in the center of the field, with an upwind fetch of grazed field across a wider band of

338 wind directions. Sensor S3 on the other hand is located at the SE field boundary, and was more limited as a

339 receptor for emissions under the prevailing northerly wind conditions. However, during NW wind directions

340 where all sensors in-line across a diagonal fetch of the field one would expect the S3 sensor to be measuring

341 similar or higher concentrations relative to S1 at the center (assuming homogenous emissions across the field),

342 which is not the case. It is also important to note that the grazing density was about 50% lower during Period 2

343 as the field was much larger.

344 Power failure led to significant data gaps from the S2 sensor and hence a loss of C_b measurements (Figure 6).

345 To fill the gaps a linear regression was applied between the measured S2 concentration and T, u, and RH.

346 However, there was considerable scatter in the data and the C_b prediction was much more uncertain than during

347 Period 1.

348
$$C_b = 2.5 - 0.1u + 0.01T - 0.02RH, \text{r2} = 0.1 \tag{6}$$

349 **3.2.2 Field-scale emissions estimates**

350 The average net emission rate (Q) from the grazed field estimated using the S1 measurements was 0.27 µg m^{-2} s^{-1}

351 while much lower emissions were estimated from the S3 measurements (0.12 µg m^{-2} s^{-1}). Both estimates show

352 a generally diurnal trend of peak emissions during the afternoon, similar to the trend observed during Period 1.

353 However, there are gaps in QS1 and QS3 overnight due to data filtering as $u*$ drops below the defined

354 threshold (0.1 m s^{-1}). Peak emissions occurred on 22/05 when the maximum concentration difference between

upwind and downwind receptors was measured. Grazing of the field ended and the cattle left the field at 15:00 GMT on 23/05. After this point a generally decreasing trend in emissions is derived from the decreasing concentrations measured by S1 and S3. There is greater uncertainty attributed to the periods without active C_b measurements marked on Figure 6.

Emission estimates from the bLS-R model were initially made on the assumption that emissions from the grazed field are spread equally (thus randomly) across a homogeneous field. However a herd of cattle can be expected to move and disperse across the field in a generally non – random way, grouping together as they graze across the field rather than acting individually. Systematic effects of uneven cattle distribution within grazed pastures have been reported previously, impacting on bLS-derived mean gaseous emissions from grazing cattle (Laubach et al., 2013b). Our measurements during Period 2 certainly support spatial heterogeneity in emissions, with higher concentrations at the centre of the field (CS1) than at the SE corner (CS3) during periods in which the wind direction was from the NW. Had the emissions been spatially homogenous, as these emissions are taken up by the atmosphere and dispersed, an increase in NH_3 concentration would have been measured with distance downwind across the NW - SE transect of the field, causing higher concentrations at S3 compared to S1.

A second set of emission estimates (Figure 6 Panel 3) were produced after optimising the emission rates from 4 separate areas (A, B, C & D, Figure 1) within the field to reproduce the observed concentrations at S1 and S3 on each measurement day. An excellent fit between QS1 and QS3 was achieved after running a numerical solver to minimise the squared error (e^2) between them. The coefficients given in Table 1 are the result of the solver, describing the spatial changes in relative emission strength over time. The solver was executed with the following conditions: (1) the sum of the area coefficients must equal 1; and (2) no area coefficient can be below 0.075. The minimum value for any area coefficient (AC_{min}) is a parameter which describes the heterogeneity of emissions, where in this case it was assumed that each source area must contribute at least 30% of the original (homogenous) value.

Henceforth the initial emission estimates calculated without applying emission area coefficients are referred to as Scenario 1 estimates, while the calculations involving heterogeneous emission area coefficients are referred to as Scenario 2 estimates. It is important to note that there can be more than one combination of coefficients to reconcile the QS1 and QS3 estimates, thus these coefficients should not be taken as definite emission strengths for each area of the field. However, they do offer a rough guide to which sections had greater emissions relative to the others, and confirm that emissions from the field were certainly not homogeneous over the course of the grazing period. The large difference in Scenario 1 QS1 and QS3 estimates may therefore be attributed to strong emissions in areas A and D, relative to C and B (Figure 1, Table 1), which explains the high measured concentrations at sensor S1 relative to S3. Emission area D represents the SW field which was grazed during Period 1, thus high emissions from this area may have been a legacy effect left by continuing emissions from cattle excretions during Period 1. Emission area D also contained a water trough which was only 15-20m away from the S1 receptor, where cattle grouping was observed. Due to the combined effects of prior grazing within the SW field and grouping around the water trough, we can expect enhanced emissions within area D. The Scenario 2 (optimised) QS1 and QS3 estimates are similar (0.19 and 0.16 µg m^{-2} s^{-1} respectively), and are believed to give a more realistic estimate of the true field-scale emission rates after accounting for spatial complexity. The data coverage for QS3 (64%) is greater than the QS1 data coverage (59%), hence some differences between QS1 and QS3 can be expected even with perfect agreement. The Q estimates can be

395 regarded as net emission rates for the grazed field, made without consideration of deposition to clean patches

396 within the source area. The Q_{dep} estimates including the effect of deposition are 16% higher (0.22 and 0.19 μg

397 m^{-2} s^{-1} for the Scenario 2 S1 and S3 estimates respectively).

3.3 Derived emission factors

399 Grazing Period 1 took place within a SW section of the field with a smaller area (5600 m^2) than the whole field

400 opened up for grazing Period 2 (19800 m^2). Although there were fewer cattle grazing during Period 1 (25) the

401 grazing density was twice as high relative to Period 2. Therefore, the higher grazing density during Period 1 is

402 consistent with the stronger emission estimates per unit area (Table 2). Emission factors (EFs) are given in

403 Table 3 for Periods 1 and 2. For both measurement periods, the S3 sensor had greater data coverage than the S1

404 sensor. Therefore, the S3 emission estimates are more representative and are selected to derive EFs. Both

405 grazing periods have produced similar emission factors of the order of 6-7 g NH$_3$ cow^{-1} d^{-1}, though there are

406 considerable differences between the two periods in terms of weather conditions and grazing timeline. Period 1

407 was shorter in length, and was characterised by steady SW/W winds, lower temperatures and wetter conditions

408 relative to Period 2 (Table 2). Therefore, the lower temperatures and wetter conditions likely limited emissions

409 (e.g. Flechard et al., 1999; Laubach et al., 2012; Móring et al., 2016).

410 The duration of Period 1 was too short to fully capture tailing emissions; excretions to the field during Period 1

411 will have continued to emit NH$_3$ during Period 2. Flux estimates are continued for 6 days after the cattle had left

412 the field during Period 2, capturing residual emissions after grazing. The combined influences of weather

413 conditions and experimental design and duration may therefore explain why a smaller fraction of excreted N and

414 urine-N was emitted as NH$_3$ during Period 1 relative to Period 2. The EFs derived from Period 2 fluxes may for

415 these reasons be considered to be more representative of the total emissions from grazing, where emissions are

416 estimated to be 6 and 7 g NH$_3$ cow^{-1} d^{-1}, and 9 and 10% excreted urine-N emitted as NH$_3$ for the Q and Q_{dep}

417 scenarios respectively. However, the greater uncertainty in Period 2 associated with missing C_b measurements

418 and heterogeneous emission patterns should be considered.

4. Discussion

4.1 Experimental design

421 Previous experiments to deduce surface-air fluxes by the bLS method have deployed sufficient measurement

422 systems so that the problem to determine C and C_b was mathematically over-determined, and the experiment

423 was not dependent on a specific range of wind directions (e.g. Flesch et al., 2014). The configuration of the

424 three miniDOAS sensors and the grazed field during Period 2 led to certain wind directions being unsuitable for

425 emission estimates, while additional miniDOAS sensors placed at field boundaries would have been beneficial.

426 However, the configuration of the miniDOAS sensors was optimised by using the weather forecast to predict the

427 wind direction prior to the grazing experiment and placing the miniDOAS sensors accordingly.

428 It was originally hypothesised that the model could treat the field area as a spatially homogenous source, where

429 emission estimates would show insensitivity to cattle grouping and excretion patterns within the field. This

430 assumption seemed valid for the Period 1 emission estimates, where very good agreement was achieved in C

431 and Q between the downwind receptors. The SW field grazed during Period 1 was smaller than the whole field

grazed during Period 2, and the wind direction was more consistent. This allowed the downwind and upwind receptors to capture the inflow and outflow concentrations and produce reliable emission estimates, while the grazing density was higher. During Period 2 the field was larger and the grazing density was 50% lower, which led to some spatial and temporal emission 'hotspots' caused by cattle grouping and/or excretions within certain areas, such as around the water trough. The S1 sensor was located very close to a 'hotspot' of emissions at the centre and SW section of the field, while the S3 sensor was located next to an area (SE corner) which appears to have seen relatively little emissions. Because of this the model could not treat the field as a homogenous source area and reconcile emission estimates between downwind receptors, and source-area differentiation (Table 1) was required. Clearly, there is a limitation in the application of the standard bLS method to estimate emissions from area sources which may not be treated as homogenous, such as pastures with a low grazing density. However, as the Period 2/Scenario 2 emission estimates demonstrate it may also be possible to account for this heterogeneity if more than one downwind concentration receptor is used and they are suitably located. Insensitivity to heterogeneous emissions has been demonstrated if concentration measurements are made at least twice as far downwind as the maximum distance between potential sources (Flesch et al., 2005). Therefore, had the miniDOAS sensors been placed differently to satisfy this criterion it is possible that no source area optimisation would have been necessary to reconcile bLS emission estimates. On the other hand, as emissions from excretions to the grazed pasture were relatively weak, at a greater distance downwind from the field the concentration rise above background may not be significant enough to evaluate the emissions.

Felber et al., (2015) applied corralling of grazing cattle into paddocks over a rotational grazing cycle to increase grazing density, and placed GPS trackers on individual cattle to attribute eddy covariance methane fluxes using a footprint model. The Period 1 emission estimates demonstrate that a smaller paddock and higher grazing density can be a solution to the heterogeneous emissions problem, however NH_3 emissions from grazing cattle arise from excretions to the field surface and are not enteric, hence GPS trackers on cattle may not track the NH_3 emissions directly as they do for methane. In order to accurately attribute fluxes from grazed pastures there is call to develop a method to track excretions spatially and temporally across a grazed field, potentially using visual observations or cameras and animal detection software. We did carry out visual observations of urination events during Period 1 (day time only), which described a fairly homogenous distribution (data not shown, Andi Móring, personal communication). Unfortunately, observations could not be carried out during Period 2.

4.2 Uncertainty in field-scale emission estimates

4.2.1 Uncertainty in miniDOAS concentration measurements and dispersion model

The instrumental uncertainty associated with the miniDOAS concentration measurements was evaluated during the initial inter-comparison phase, where the systems were configured to measure in parallel. Very good agreement was observed between the analysers, with a slope of one and an intercept close to zero. Deviations between the S1, S2 and S3 analysers were minor, and the coefficient of variation between them was determined to be 3.4% (unpublished data). Sintermann et al., (2016) have described this inter-comparison phase and the miniDOAS performance in detail, however the authors compare only the miniDOAS sensors S2 and S3 as these sensors were fitted with all of the updated Swiss miniDOAS instrumental features discussed within that study.

Since the input data had been filtered to remove conditions which do not meet the established criteria ($u* < 0.1$ m s^{-1}), and instrumental uncertainty associated with the concentration measurements is very low, the principal

471 uncertainties are associated with the modelled results, principally the input variables which could not be
472 measured directly, such as R_c, and the predicted background concentration C_b used for gap-filling.
473 The bLS dispersion model theory has been well validated in past experiments (e.g. Flesch et al., 2004; McGinn
474 et al. 2009), however we can assume a general overall uncertainty based on evaluated performance by an
475 ensemble of published trace gas release experiments. A review of 24 bLS tracer release assessments (Häni et al.,
476 2016) found that the uncertainty is generally between 10 and 20% for the bLS method.

4.2.2 Uncertainty in background concentration

478 The background concentration (C_b) had to be predicted to "fill in" the gaps in the C_b measurements upwind of
479 the field measured by miniDOAS sensor S2. Multiple regression equations (Eq. 5; 6) were based on previous
480 observations that background NH_3 is dependent on wind speed, temperature and relative humidity (Flechard and
481 Fowler, 1998), but nonetheless error is introduced due to differences between the predicted C_b and the actual C_b.
482 The mean absolute error (MAE) between the measured and predicted C_b for Periods 1 and 2 have been applied
483 to offset to the predicted C_b timeseries input to the model, to determine the limits (upper and lower) of emission
484 estimates caused by this uncertainty. The MAE between the observed and predicted background concentrations
485 during Period 1 was 0.33 µg m^{-3}, while the percentage of data coverage (observed C_b measurements) was 67%.
486 Measurement Period 2 had a greater MAE between observed and predicted C_b (0.56 µg m^{-3}) (Table 4), as the
487 multiple regression equation used to fill (C_b) measurement gaps did not give very accurate predictions (Eq. 6).
488 Furthermore, the upwind sensor S2 was only active during 44% of the measurement period; therefore the Period
489 2 emission estimates are more sensitive to this uncertainty. The % change in Q_{dep} to predicted C_b ± MAE was
490 much greater during Period 2 (± 31%) than Period 1 (± 5%).

4.2.3 Uncertainty in local dry deposition of field-emitted NH_3

492 The inclusion of dry deposition within the bLS-R model is intended to simulate the deposition of NH_3 to the
493 surface of 'clean' grass patches within the grazed field. This process is described by a resistance model, and
494 while the R_a and R_b components may be derived directly from eddy covariance measurements, as well as well-
495 established models, the R_c component is empirical. In this case, the empirical R_c model (Eq. 4) was derived
496 from a curve fitting exercise of time-integrated COTAG flux measurement to meteorological variables T and
497 RH. The R_c model is based on a long (1.5 years) series of measurements taken from the field (deposition periods
498 only), while the effect of soiled grass areas on R_c during grazing is also approximated using the 130 s m^{-1} R_c
499 offset within the Q_{dep} scenario. It is conceivable that there is significant error (up to 50%) in estimating R_c by
500 this method. The sensitivity of the bLS-R model to potential uncertainty within the R_c estimates has been
501 evaluated, where the R_c timeseries has been varied by factors of plus and minus 50%. The results of this
502 sensitivity test are given in Table 4. The % change in Q_{dep} after varying R_c by ± 50% was -4% and +12% for
503 Period 1 and ± 5% for Period 2.
504 While impact of this uncertainty on the absolute value for Q_{dep} is not very large, the change in Q_{dep} relative to
505 Q is significant. The Period 2 Q_{dep} uncertainty due to predicted R_c is ± 5%; therefore including deposition in the
506 model has increased Q_{dep} above Q by 16 ± 6%. Alternatively, we can say that 14 ± 4% of NH_3 emitted from
507 excretions had been re-deposited to clean patches on the field.

4.2.4 Uncertainty associated with heterogeneous emission patterns

To address the resulting disparity between emission estimates from the downwind concentration receptors during Period 2, the emission area coefficients (Table 1) were applied to reconcile the independent emission estimates. This is a valid approach to describe emissions from the field as a whole, as sensor S1 was placed at the center of the field near the strongest area of emissions, causing emissions to be overestimated as a whole, while the field area around sensor S3 at the SE corner seems to have contributing very little emissions, hence causing an underestimation. However, as mentioned previously there are multiple configurations of source area coefficients which can reconcile $QS1$ and $QS3$. Therefore, a sensitivity test has been carried out to evaluate the potential error in this method. The numerical solver which derives the source area coefficients contains a parameter assuming the maximum degree of heterogeneity for the field, where each source area cannot contribute less than a defined percentage to the overall emissions. This parameter (AC_{min}) was varied to provide differing sets of source area coefficients, yet still reconciling the $QS1$ and $QS3$ emission estimates which was a necessary precondition for the sensitivity test. AC_{min} was initially assumed be 0.075, 30% of the value for a homogenous field (0.25), and this value was varied by ± 67% (to 50% and 10% of the homogenous value). The results of this sensitivity test are given in Table 4, where the percentage change in Q_{dep} after varying the parameter by +67% and -67% was 9 and 1, respectively. The percentage change is greater after increasing AC_{min} because $QS1$ and $QS3$ cannot be reconciled as closely, whereas decreasing AC_{min} from 0.075 leads to very little change as the numerical solver can find very close agreement. This suggests that emissions from excretions to the field are too heterogeneous to assume an AC_{min} value of 0.125 (50% of homogeneous value), and that the 1% change in Q_{dep} after reducing AC_{min} to 0.025 (10% of homogeneous value) is more indicative of the uncertainty in the source area optimisation method.

The % change in emission estimates was much more sensitive to uncertainty in predicted C_b than to uncertainty in R_c or AC_{min}. Therefore, we expect that the predicted C_b is the greatest source of error in derived fluxes from the grazed field.

4.3 Temporal variability in estimated emissions

The estimated emissions show significant temporal variability during both measurement periods, typically with peak emissions occurring during the day with little emissions occurring overnight. Similar diurnal profiles have been observed in NH_3 emissions from cattle urine and dung patches (Laubach et al., 2012; 2013a), and from urine patch emission models (Móring et al., 2016). Mechanisms which limit nocturnal emissions can be summarised as: (1) low wind speeds and stable conditions, which increases the aerodynamic transfer resistances between the soil/canopy layer and the atmosphere, (2) low temperatures which limit the hydrolysis of urea, and affect NH_3/NH_4^+ partitioning in solutions, (3) dew formation on leaf surfaces which act as sinks for NH_3.

A longer temporal trend in emissions is observed during Period 1; with very little emissions occurring on the first day the cattle were introduced to the field, and peak emissions occurring during the afternoon of the second day. After 44 cattle had begun to graze the whole field during Period 2, peak emission rates occurred from 22-23/05, 2-3 days after the cattle had been introduced. A decreasing trend in emissions occurred after the cattle were removed from the field on 23/05 until the end of the measurement period. This is in-line with the reported emissions from urine and dung patches by Laubach et al., (2013a), where emissions peaked during the third and

546 fourth days after grazing had begun, and a following decreasing trend in emissions after the cattle had been
547 removed from the field on the third day.

548 The peak in emissions which occurred during grazing can be attributed to the hydrolysis of urea within the urine
549 patches, which leads to a rapid rise in pH and the formation of NH_4^+, and a high rate of NH_3 volatilisation
550 (Sherlock and, Goh 1985). As volatilisation proceeds, a subsequent chemical reduction in surface pH occurs
551 with an accompanying release of a proton to the transformation of NH_4^+ to NH_3 (Laubach et al., 2012; Sherlock
552 and Goh, 1985, Móring, et al.. 2016), which prevents further volatilisation and can explain the declining
553 emission rate after the cattle had left the field on 23/05.

4.4 Emission factors from the grazing experiment

555 Emission factors from the grazing experiment have been evaluated as 6 ± 2 and 7 ± 2 g NH_3 cow^{-1} d^{-1}, and $9 \pm$
556 3% and $10 \pm 3\%$ of excreted urine-N emitted as NH_3 for the Q and Q_{dep} scenarios respectively (average
557 emission factor $\pm$ predicted C_b uncertainty). These emission factors were taken from the Period 2/Scenario 2
558 estimates as the measurements carried out during Period 1 did not capture the residual emissions which occurred
559 after the cattle had left the field. The Period 1 & 2 emission estimates were derived from very different
560 experimental conditions (particularly wetness & grazing density), therefore we may not combine the two periods
561 into a single emission factor. Previous experiments have measured NH_3 emissions from cattle urine patches at
562 ratios of 7-25.7% of excreted urine-N to grazed pastures (Jarvis et al., 1989; Ryden et al., 1987; Laubach et al.,
563 2012; 2013a). Our estimates for emissions from grazing are towards the lower end of the range of published
564 emission factors. Differences between reported emission factors may be related to differing weather conditions
565 affecting the hydrolysis of urea, or differences in soil properties, where emissions can be limited due to urine
566 percolation into porous soil (Móring et al., 2016). It is also possible that significant emissions occurred after the
567 miniDOAS instruments had been removed from the field, which would lead to an underestimation of the
568 proportion of excreted N or urine-N emitted as NH_3. The period of significant emissions from urine patches
569 generally lasts 4-8 days after urine deposition (Sherlock and Goh, 1985; Laubach et al., 2012). However, a
570 rainfall event after a dry period can lead to a delayed onset of NH_3 emissions by restarting urea hydrolysis
571 (Móring et al., 2016). On the other hand, the Period 2 emission factors are also influenced to some degree by
572 emissions from excretions during Period 1 on the SW field, which could cause an overestimation of emissions.
573 Emission factors derived from Period 2 are also affected by $u*$ filtering, which may slightly increase estimates
574 due to a measurement bias towards turbulent daytime periods.

575 The emission estimates presented here show that the 'gross' emissions from the field (Q_{dep} scenario) are around
576 $16 \pm 6\%$ higher than the 'net' emissions (Q scenario). Both of these estimates are potentially useful to contribute
577 towards an emission factor for livestock grazing. For example, regional-scale atmospheric dispersion models
578 may require source inputs as 'gross' emission factors due to deposition simulations implicit within the regional-
579 scale model.

5. Conclusion

581 Fluxes of NH_3 were estimated through measurement of atmospheric concentrations upwind and downwind of a
582 grazed field, and applying a bLS dispersion model to simulate the emission rate on a half hourly basis from the

observed horizontal concentration gradient and wind/turbulence measurements. The miniDOAS systems were well-suited to the task, providing continuous high-time resolution concentration measurements at field boundaries across the field. Horizontal concentration gradients of ~0-9 $\mu g\ m^{-3}$ were measured between upwind and downwind receptors. Control on emissions was observed from covariance with temperature, wind speed and humidity/wetness measurements made on the field, revealing a diurnal emission profile. Two separate experiments to evaluate emissions were carried out; a Period 1 experiment (2 days) which took place on a small field with a grazing density of 44 cows ha^{-1}, and a Period 2 experiment (10 days) on a larger field with a grazing density of 22 cows ha^{-1}. Spatial heterogeneity in emissions across the field was apparent during Period 2, because of uneven cattle distribution and a low grazing density, adversely affecting the accuracy of the bLS model estimates. However, after treating the larger field as a grid of discrete source areas the spatial heterogeneity of emissions was accounted for, by optimising source area coefficients to the measured concentrations and reconciling emission estimates between downwind receptors.

Data gaps in the C_b measurements were filled by applying linear regression equations with u, T and RH, which introduced significant uncertainty into the emission estimates. The evaluated uncertainty in derived emissions due to C_b gap-filling was 5% during Period 1 and 31% during Period 2.

In contrast to the standard bLS approach, we simulated the effect of re-deposition to unsoiled field patches, where the canopy resistance (R_c) component was estimated by an empirical model derived from local flux and R_c measurements with T and RH. Including deposition in the model increased emissions by 16 ± 6%. The results present both 'gross' and 'net' emissions from the field, and show that deposition of NH_3 is an important consideration when deriving NH_3 emission factors.

Acknowledgements

This study was undertaken as part of the French BtEP project (Emissions gazeuses au Bâtiment, sTockage, Epandage et Pâturage des systèmes bovins laitiers), convention n° 1360C0032, with funding provided by ADEME (Agence de l'environnement et de la maîtrise de l'énergie). We are thankful to Région Bretagne regional council for PhD grant co-funding under the ARED scheme. We wish to thank David Sidaner, Jacques Lassalas and all of the staff at the INRA-Méjusseaume dairy experimental farm. We wish to thank Andi Móring for assistance during the measurement campaign. We wish to thank Thomas Kupper for organising the setup of the N excretion model.

Competing interests

The authors declare that they have no conflict of interest.

References

Asman, W. A. H.: Factors influencing local dry deposition of gases with special reference to ammonia, Atmospheric Environment, 32, 415-421, Doi 10.1016/S1352-2310(97)00166-0, 1998.

Asman, W. A. H., Sutton, M. A., and Schjorring, J. K.: Ammonia: emission, atmospheric transport and deposition, New Phytol, 139, 27-48, DOI 10.1046/j.1469-8137.1998.00180.x, 1998.

618 Bracher A., Schlegel P., Münger A., Stoll W., Menzi H., 2011. Möglichkeiten zur Reduktion von
619 Ammoniakemissionen durch Fütterungsmassnahmen beim Rindvieh (Milchkuh). Project report Schweizerische
620 Hochschule für Landwirtschaft and Agroscope Liebefeld-Posieux for the Swiss Federal Office of Agriculture,
621 pp. 128, available at: https://www.blw.admin.ch/blw/de/home/instrumente/ressourcen--und-
622 gewaesserschutzprogramm/ressourcenprogramm.html, last access: 4 October 2016.

623 Bracher A., Spring P., Münger A., Schlegel P., Stoll W., Menzi H., 2012. Feeding measures to reduce ammonia
624 emissions. Hassouna M. et al. (Eds), Proc. International Symposium on Emissions of Gas and Dust from
625 Livestock (EMILI), Saint-Malo 11-13.6.2012, p. 39.

626 Carslaw, D. C., and Ropkins, K.: openair - An R package for air quality data analysis, Environ Modell Softw,
627 27-28, 52-61, 10.1016/j.envsoft.2011.09.008, 2012.

628 Erisman, J. W., Sutton, M. A., Galloway, J., Klimont, Z., and Winiwarter, W.: How a century of ammonia
629 synthesis changed the world, Nat Geosci, 1, 636-639, 10.1038/ngeo325, 2008.

630 Famulari, D., Fowler, D., Nemitz, E., Hargreaves, K. J., Storeton-West, R. L., Rutherford, G., Tang, Y. S.,
631 Sutton, M. A., and Weston, K. J.: Development of a low-cost system for measuring conditional time-averaged
632 gradients of SO2 and NH3, Environmental Monitoring and Assessment, 161, 11-27, 10.1007/s10661-008-0723-
633 6, 2010.

634 Felber, R., Munger, A., Neftel, A., and Ammann, C.: Eddy covariance methane flux measurements over a
635 grazed pasture: effect of cows as moving point sources, Biogeosciences, 12, 3925-3940, 10.5194/bg-12-3925-
636 2015, 2015.

637 Flechard, C. R., and Fowler, D.: Atmospheric ammonia at a moorland site. I: The meteorological control of
638 ambient ammonia concentrations and the influence of local sources, Q J Roy Meteor Soc, 124, 733-757, DOI
639 10.1002/qj.49712454705, 1998.

640 Flechard, C. R., Fowler, D., Sutton, M. A., and Cape, J. N.: A dynamic chemical model of bi-directional
641 ammonia exchange between semi-natural vegetation and the atmosphere, Q J Roy Meteor Soc, 125, 2611-2641,
642 DOI 10.1002/qj.49712555914, 1999.

643 Flechard, C. R., Spirig, C., Neftel, A., and Ammann, C.: The annual ammonia budget of fertilised cut grassland
644 - Part 2: Seasonal variations and compensation point modeling, Biogeosciences, 7, 537-556, 2010.

645 Flechard, C. R., Massad, R. S., Loubet, B., Personne, E., Simpson, D., Bash, J. O., Cooter, E. J., Nemitz, E., and
646 Sutton, M. A.: Advances in understanding, models and parameterizations of biosphere-atmosphere ammonia
647 exchange, Biogeosciences, 10, 5183-5225, 10.5194/bg-10-5183-2013, 2013.

648 Flesch, T. K., Wilson, J. D., and Yee, E.: Backward-Time Lagrangian Stochastic Dispersion Models and Their
649 Application to Estimate Gaseous Emissions, J Appl Meteorol, 34, 1320-1332, Doi 10.1175/1520-
650 0450(1995)034<1320:Btlsdm>2.0.Co;2, 1995.

651 Flesch, T. K., Wilson, J. D., Harper, L. A., Crenna, B. P., and Sharpe, R. R.: Deducing ground-to-air emissions
652 from observed trace gas concentrations: A field trial, J Appl Meteorol, 43, 487-502, Doi 10.1175/1520-
653 0450(2004)043<0487:Dgefot>2.0.Co;2, 2004.

654 Flesch, T. K., Wilson, J. D., Harper, L. A., and Crenna, B. P.: Estimating gas emissions from a farm with an
655 inverse-dispersion technique, Atmospheric Environment, 39, 4863-4874, 10.1016/j.atmosenv.2005.04.032,
656 2005.

657   Flesch, T. K., McGinn, S. M., Chen, D., Wilson, J. D., and Desjardins, R. L.: Data filtering for inverse

658   dispersion emission calculations, Agr Forest Meteorol, 198, 1-6, 10.1016/j.agrformet.2014.07.010, 2014.

659   Fowler, D., Pilegaard, K., Sutton, M. A., Ambus, P., Raivonen, M., Duyzer, J., Simpson, D., Fagerli, H., Fuzzi,

660   S., Schjoerring, J. K., Granier, C., Neftel, A., Isaksen, I. S. A., Laj, P., Maione, M., Monks, P. S., Burkhardt, J.,

661   Daemmgen, U., Neirynck, J., Personne, E., Wichink-Kruit, R., Butterbach-Bahl, K., Flechard, C., Tuovinen, J.

662   P., Coyle, M., Gerosa, G., Loubet, B., Altimir, N., Gruenhage, L., Ammann, C., Cieslik, S., Paoletti, E.,

663   Mikkelsen, T. N., Ro-Poulsen, H., Cellier, P., Cape, J. N., Horvath, L., Loreto, F., Niinemets, U., Palmer, P. I.,

664   Rinne, J., Misztal, P., Nemitz, E., Nilsson, D., Pryor, S., Gallagher, M. W., Vesala, T., Skiba, U., Brueggemann,

665   N., Zechmeister-Boltenstern, S., Williams, J., O'Dowd, C., Facchini, M. C., de Leeuw, G., Flossman, A.,

666   Chaumerliac, N., and Erisman, J. W.: Atmospheric composition change: Ecosystems-Atmosphere interactions,

667   Atmospheric Environment, 43, 5193-5267, 10.1016/j.atmosenv.2009.07.068, 2009.

668   Gao, Z. L., Mauder, M., Desjardins, R. L., Flesch, T. K., and van Haarlem, R. P.: Assessment of the backward

669   Lagrangian Stochastic dispersion technique for continuous measurements of CH4 emissions, Agr Forest

670   Meteorol, 149, 1516-1523, 10.1016/j.agrformet.2009.04.004, 2009.

671   Genermont, S., and Cellier, P.: A mechanistic model for estimating ammonia volatilization from slurry applied

672   to bare soil, Agr Forest Meteorol, 88, 145-167, Doi 10.1016/S0168-1923(97)00044-0, 1997.

673   Gill Instruments: Technical key note KN1509v3* - software bug affecting 'w' wind component notice and

674   available   options   to   customers   –   February   2016,   available   at:

675   http://gillinstruments.com/data/manuals/KN1509_WindMaster_WBug_info.pdf, last access: 4 October 2016.

676   Häni, C.: bLSmodelR - An atmospheric dispersion model in R. R package version 2.4.1. URL:

677   http://www.agrammon.ch/documents-to-download/blsmodelr/, last access: 22 September 2016.

678   Häni, C., Sintermann, J., Jocher, M., Neftel, A.: Ammonia emissions after application of slurry. pp. 168.

679   Hochschule   für   Agrar-,   Forst-   und   Lebensmittelwissenschaften,   HAFL,   Agroscope   Institut   für

680   Nachhaltigkeitswissenschaften   INH,   available   at:

681   http://www.agrammon.ch/assets/Downloads/SchlussberichtInklAnh20160728subm.pdf, last access: 4 October

682   2016.

683   Harper, L. A., Denmead, O. T., and Flesch, T. K.: Micrometeorological techniques for measurement of enteric

684   greenhouse gas emissions, Anim Feed Sci Tech, 166-67, 227-239, 10.1016/j.anifeedsci.2011.04.013, 2011.

685   Hertel, O., Reis, S., Skjøth, C. A., Bleeker, A., Harrison, R., Cape, J. N., Fowler, D., Skiba, U., Simpson, D.,

686   Jickells, T., Baker, A., Kulmala, M., Gyldenkaerne, S., Sørensen, L. L., and Erisman, J. W.:, 2011. Nitrogen

687   processes in the atmosphere, in: The European Nitrogen Assessment – Sources, Effects and Policy Perspectives,

688   edited by Sutton, M. A., Howard, C. M., Erisman, J. W., Billen, G., Grennfelt, P., van Grinsven, H., and

689   Grizzetti, B., 177–207, Cambridge University Press, Cambridge, UK, 2011.

690   Kruit, R. J. W., van Pul, W. A. J., Sauter, F. J., van den Broek, M., Nemitz, E., Sutton, M. A., Krol, M., and

691   Holtslag, A. A. M.: Modeling the surface-atmosphere exchange of ammonia, Atmospheric Environment, 44,

692   945-957, 10.1016/j.atmosenv.2009.11.049, 2010.

693   Hutchings, N. J., Sommer, S. G., Andersen, J. M., and Asman, W. A. H.: A detailed ammonia emission

694   inventory for Denmark, Atmospheric Environment, 35, 1959-1968, Doi 10.1016/S1352-2310(00)00542-2, 2001.

695   Jarvis, S. C., Hatch, D. J., and Roberts, D. H.: The Effects of Grassland Management on Nitrogen Losses from

696   Grazed Swards through Ammonia Volatilization - the Relationship to Excretal-N Returns from Cattle, J Agr Sci,

697   112, 205-216, 1989.

698   Laubach, J., Taghizadeh-Toosi, A., Sherlock, R. R., and Kelliher, F. M.: Measuring and modelling ammonia

699   emissions from a regular pattern of cattle urine patches, Agr Forest Meteorol, 156, 1-17,

700   10.1016/j.agrformet.2011.12.007, 2012.

701   Laubach, J., Taghizadeh-Toosi, A., Gibbs, S. J., Sherlock, R. R., Kelliher, F. M., and Grover, S. P. P.: Ammonia

702   emissions from cattle urine and dung excreted on pasture, Biogeosciences, 10, 327-338, 10.5194/bg-10-327-

703   2013, 2013a.

704   Laubach, J., Bai, M., Pinares-Patino, C. S., Phillips, F. A., Naylor, T. A., Molano, G., Rocha, E. A. C., and

705   Griffith, D. W. T.: Accuracy of micrometeorological techniques for detecting a change in methane emissions

706   from a herd of cattle, Agr Forest Meteorol, 176, 50-63, 10.1016/j.agrformet.2013.03.006, 2013b.

707   Loubet, B., Cellier, P., Milford, C., and Sutton, M. A.: A coupled dispersion and exchange model for short-

708   range dry deposition of atmospheric ammonia, Q J Roy Meteor Soc, 132, 1733-1763, 10.1256/qj.05.73, 2006.

709   Loubet, B., Asman, W. A. H., Theobald, M. R., Hertel, O., Tang, Y. S., Robin, P., Hassouna, M., Dammgen, U.,

710   Genermont, S., Cellier, P., and Sutton, M. A.: Ammonia Deposition Near Hot Spots: Processes, Models and

711   Monitoring Methods, Atmospheric Ammonia, 205-267, Doi 10.1007/978-1-4020-9121-6_15, 2009.

712   McGinn, S. M., Beauchemin, K. A., Flesch, T. K., and Coates, T.: Performance of a Dispersion Model to

713   Estimate Methane Loss from Cattle in Pens, J Environ Qual, 38, 1796-1802, 10.2134/jeq2008.0531, 2009.

714   Menzi H., Huguenin O., Muenger A., Schlegel P. Procedure for defining new Swiss standard values for the

715   nutrient excretions of dairy cows. In Koerner I. et al. (Eds.), Proc. 16th RAMIRAN Conference, Hamburg

716   Harburg September 8-10 2015, Book of Abstracts, p. 52, 2015.

717   Móring, A., Vieno, M., Doherty, R. M., Laubach, J., Taghizadeh-Toosi, A., and Sutton, M. A.: A process-based

718   model for ammonia emission from urine patches, GAG (Generation of Ammonia from Grazing): description and

719   sensitivity analysis, Biogeosciences, 13, 1837-1861, 10.5194/bg-13-1837-2016, 2016.

720   Pain, B. F., Van der Weerden, T. J., Chambers, B. J., Phillips, V. R., and Jarvis, S. C.: A new inventory for

721   ammonia emissions from UK agriculture, Atmospheric Environment, 32, 309-313, Doi 10.1016/S1352-

722   2310(96)00352-4, 1998.

723   R Core Team: R: A language and environment for statistical computing. R Foundation for Statistical

724   Computing, Vienna, Austria, available at: https://www.R-project.org/, last access: 04 October 2016.

725   Reidy, B., Dammgen, U., Dohler, H., Eurich-Menden, B., van Evert, F. K., Hutchings, N. J., Luesink, H. H.,

726   Menzi, H., Misselbrook, T. H., Monteny, G. J., and Webb, J.: Comparison of models used for national

727   agricultural ammonia emission inventories in Europe: Liquid manure systems, Atmospheric Environment, 42,

728   3452-3464, 10.1016/j.atmosenv.2007.04.009, 2008.

729   Ryden, J. C., Whitehead, D. C., Lockyer, D. R., Thompson, R. B., Skinner, J. H., and Garwood, E. A.:

730   Ammonia Emission from Grassland and Livestock Production Systems in the Uk, Environ. Pollut., 48, 173-184,

731   Doi 10.1016/0269-7491(87)90032-7, 1987.

732   Sherlock, R. R., and Goh, K. M.: Dynamics of Ammonia Volatilization from Simulated Urine Patches and

733   Aqueous Urea Applied to Pasture .1. Field Experiments, Fert Res, 5, 181-195, Doi 10.1007/Bf01052715, 1984.

734 Sherlock, R. R., and Goh, K. M.: Dynamics of Ammonia Volatilization from Simulated Urine Patches and
735 Aqueous Urea Applied to Pasture .2. Theoretical Derivation of a Simplified Model, Fert Res, 6, 3-22, Doi
736 10.1007/Bf01058161, 1985.

737 Sintermann, J., Neftel, A., Ammann, C., Hani, C., Hensen, A., Loubet, B., and Flechard, C. R.: Are ammonia
738 emissions from field-applied slurry substantially over-estimated in European emission inventories?,
739 Biogeosciences, 9, 1611-1632, 10.5194/bg-9-1611-2012, 2012.

740 Sintermann, J., Dietrich, K., Hani, C., Bell, M., Jocher, M., and Neftel, A.: A miniDOAS instrument optimised
741 for ammonia field measurements, Atmos Meas Tech, 9, 2721-2734, 10.5194/amt-9-2721-2016, 2016.

742 Sommer, S. G., Sogaard, H. T., Moller, H. B., and Morsing, S.: Ammonia volatilization from sows on grassland,
743 Atmospheric Environment, 35, 2023-2032, Doi 10.1016/S1352-2310(00)00428-3, 2001.

744 Sutton, M. A., Fowler, D., and Moncrieff, J. B.: The Exchange of Atmospheric Ammonia with Vegetated
745 Surfaces .1. Unfertilized Vegetation, Q J Roy Meteor Soc, 119, 1023-1045, DOI 10.1002/qj.49711951309,
746 1993.

747 Sutton, M. A., Howard, C. M., Erisman, J.W., Bealey,W. J., Billen, G., Bleeker, A., Bouwman, A. F., Grennfelt,
748 P., van Grinsven, H. and Grizzetti, B.: The challenge to integrate nitrogen science and policies: the European
749 Nitrogen Assessment approach, in: The European Nitrogen Assessment: Sources, Effects and Policy
750 Perspectives, edited by: Sutton, M. A., Howard, C. M., Erisman, J. W., Billen, G., Bleeker, A., Grennfelt, P.,
751 van Grinsven, H., and Grizzetti, B., Cambridge University Press, Cambridge, ISBN 978-1-107-00612-6, 82-96,
752 2011.

753 Tang, Y. S., Cape, J. N. and Sutton, M. A.: Development and Types of Passive Samplers for 570 Monitoring
754 Atmospheric NO2 and NH3 Concentrations, Sci. World, 1, 513–529, Doi:10.1100/tsw.2001.82, 2001.

755 Volten, H., Bergwerff, J. B., Haaima, M., Lolkema, D. E., Berkhout, A. J. C., van der Hoff, G. R., Potma, C. J.
756 M., Kruit, R. J. W., van Pul, W. A. J., and Swart, D. P. J.: Two instruments based on differential optical
757 absorption spectroscopy (DOAS) to measure accurate ammonia concentrations in the atmosphere, Atmos Meas
758 Tech, 5, 413-427, 10.5194/amt-5-413-2012, 2012.

759 von Bobrutzki, K., Braban, C. F., Famulari, D., Jones, S. K., Blackall, T., Smith, T. E. L., Blom, M., Coe, H.,
760 Gallagher, M., Ghalaieny, M., McGillen, M. R., Percival, C. J., Whitehead, J. D., Ellis, R., Murphy, J., Mohacsi,
761 A., Pogany, A., Junninen, H., Rantanen, S., Sutton, M. A., and Nemitz, E.: Field inter-comparison of eleven
762 atmospheric ammonia measurement techniques, Atmos Meas Tech, 3, 91-112, 10.5194/amt-3-91-2010, 2010.

763 Whitehead, D. C.: Grassland Nitrogen. CAB International, Wallingford, UK, 1995.

764 Wesely, M. L., and Hicks, B. B.: A review of the current status of knowledge on dry deposition, Atmospheric
765 Environment, 34, 2261-2282, Doi 10.1016/S1352-2310(99)00467-7, 2000.

766 Zaman, M., Saggar, S., Blennerhassett, J. D., and Singh, J.: Effect of urease and nitrification inhibitors on N
767 transformation, gaseous emissions of ammonia and nitrous oxide, pasture yield and N uptake in grazed pasture
768 system, Soil Biol Biochem, 41, 1270-1280, 10.1016/j.soilbio.2009.03.011, 2009.

769
770
771
772
773

774 **Tables**

775 **Table 1: Series of emission coefficients obtained by numerical solving of the difference between $QS1$ and $QS3$,**
776 **applied to individual emission areas to fit the bLS-R model to concentration measurements on each day. For a grazed**
777 **field with homogeneous emissions the emission coefficients for each area would be 0.25. Therefore the emission**
778 **coefficients offset the bias in emission estimates between the sensors S1 and S3 by adjusting to the heterogeneity in**
779 **emissions across the field area.**

Emission area	20/05	21/05	22/05	23/05	24/05	25/05	26/05	27/05	28/05	29/05
A	0.56	0.31	0.28	0.56	0.36	0.42	0.26	0.21	0.25	0.17
B	0.08	0.14	0.13	0.17	0.18	0.17	0.25	0.25	0.23	0.25
C	0.07	0.07	0.20	0.09	0.19	0.11	0.23	0.28	0.21	0.27
D	0.29	0.47	0.40	0.18	0.26	0.30	0.27	0.26	0.31	0.31

780

Table 2: Summary table of measurement and modelling results.

	Period 1			Period 2		
	Scenario[1]	S1	S3	Scenario	S1	S3
$C - C_b$ (µg NH$_3$ m^{-3})		1.4	2.1		2.9	1.2
Q (µg NH$_3$ m^{-2} s^{-1})		0.27	0.29	1	0.27	0.12
				2	0.19	0.16
Q_{dep} (µg NH$_3$ m^{-2} s^{-1})		0.31	0.34	1	0.31	0.14
				2	0.22	0.19
Q_{depmax} (µg NH$_3$ m^{-2} s^{-1})		0.33	0.38	1	0.33	0.14
				2	0.24	0.2
T (°C)		10			14	
u (m s^{-1})		2			1.2	
RH (%)		77			76	
Total Rain (mm)		4.4			0	
LW (% time wet)		84			40	
R_c (s m^{-1})	Q_{depmax}	145		Q_{depmax}	208	
	Q_{dep}	275		Q_{dep}	338	
v_d (mm s^{-1})	Q_{depmax}	4.4		Q_{depmax}	3.2	
	Q_{dep}	2.8		Q_{dep}	2.2	

[1]Description of model scenarios: Q_{dep} is the bLS-R emission estimate including dry deposition, with an offset of 130 s m^{-1} applied to the R_c timeseries to account for the limiting of excreted NH$_3$ to deposition. Q_{depmax} is the emission estimate without the offset applied to the R_c timeseries, and is hence a maximum prediction of the gross emissions from the field. Period 2 emission estimates contain both the original Scenario 1 emission estimates assuming a homogenous field, and the optimised Scenario 2 emission estimates using the area coefficients given in Table 1.

Table 3: N excretion model inputs, results, and derived emission factors

Model Input	Value		Model Output or Emission Factor[1]	Scenario[2]	Value	
	Period 1	Period 2			Period 1	Period 2
Animal Numbers	25	44	N excretion total (kg)		11	40
Animal weight (kg)	650	650	N excretion urine (kg)		8	28
Days since calving	180	183	N excretion faeces (kg)		3	12
Milk yield (kg cow^{-1} day^{-1})	21	22	EF (% total excreted N emitted as NH$_3$)	Q	2.5	5.2
				Q_{dep}	2.9	6
Grass sward: net energy for lactation (MJ kg DM^{-1})	6.4	6.4	EF (% total excreted urine-N emitted as NH$_3$)	Q	2.9	8.9
				Q_{dep}	4.2	10.4
Grass sward: crude protein content (g kg DM^{-1})	168	168	EF (g NH$_3$ cow^{-1} d^{-1})	Q	5.7	6.2
				Q_{dep}	6.5	7.2

[1]N excretion calculations are given as the herd total for each measurement period.

[2]Q is the net emission rate derived without including deposition in the bLS-R simulation, Q_{dep} is the gross bLS-R emission estimate including dry deposition, with an R_c offset of 130 s m^{-1}. EFs are derived from the S3 flux estimates due to better data coverage during both measurement periods, and Period 2 fluxes are derived from Scenario 2 estimates.

Table 4: Sensitivity analysis of the percentage change of the bLS-R gross emission estimates (Q_{dep}) to variation in predicted C_b and R_c, and the source area coefficient parameter AC_{min}.

	Period 1	Period 2
C_b data coverage (%)	67	44
C_b MAE (µg m^{-3})	0.33	0.56
% Change $C_b \pm$ MAE[1]	-5% +5%	-31% +31%
% Change $R_c \pm$ 20%	-2% +3%	-3% +3%
% Change $R_c \pm$ 50%	-4% +12%	-5% +5%
% Change $AC_{min} \pm$ 67%[2]	-	-9% -1%

[1]The predicted C_b timeseries input to the bLS-R model is varied by the Mean Absolute Error (MAE) between the measured and predicted C_b. The first value in all cases the % change + variation and the second the % change – variation.

[2] The percentage change in Q_{dep} is given after varying the source area coefficient parameter AC_{min} by 67% (0.075 ± 0.05).
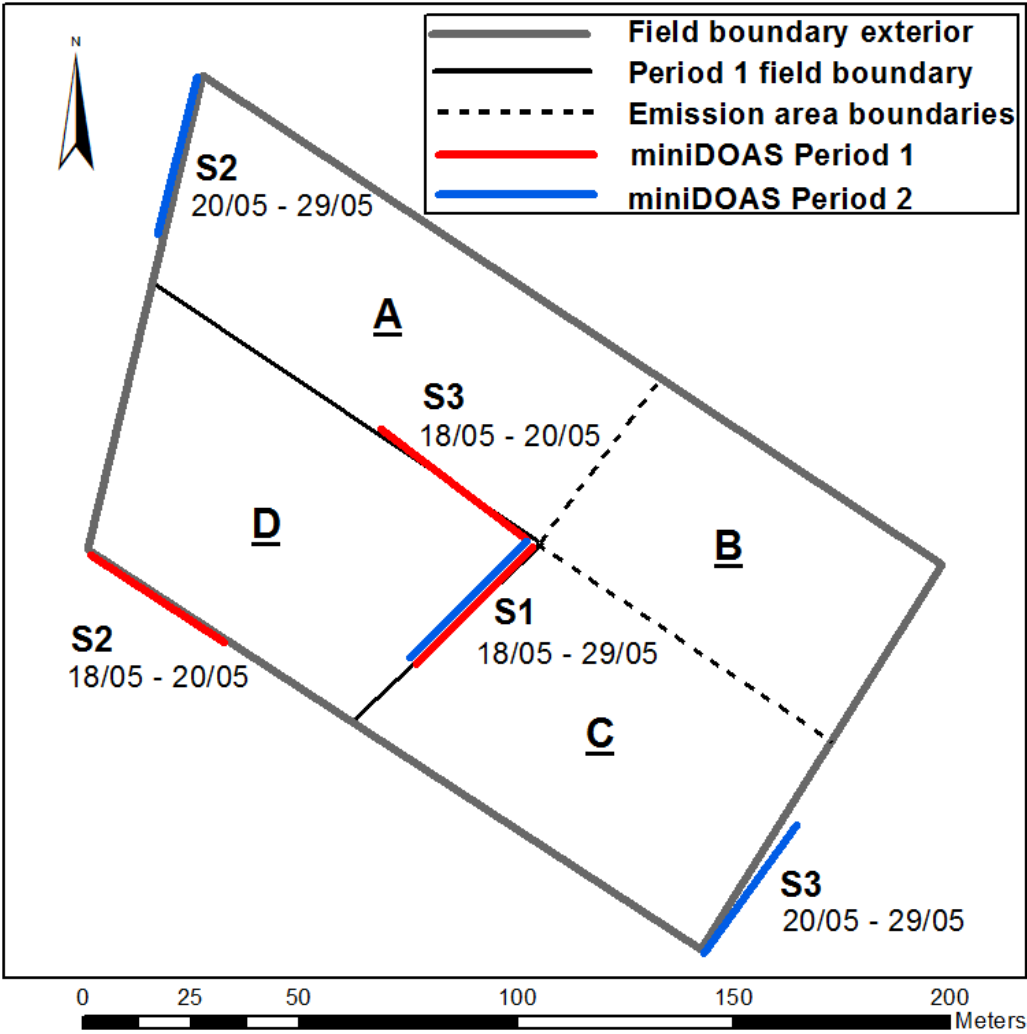
Figures

799
800 **Figure 1: Map of the grazed field showing positions of the three miniDOAS open-path measurement systems. During**
801 **Period 1 (18-20/05) 25 cattle were fenced within the SW field section (area D). During Period 2 (20-29/05) the internal**
802 **field boundaries were removed so that the cattle could graze the whole field. Later, for the attribution of emissions**
803 **across the field, emission area quadrants have been allocated, marked A-D. There were no physical barriers between**
804 **the emission areas during Period 2.**

805

806

807
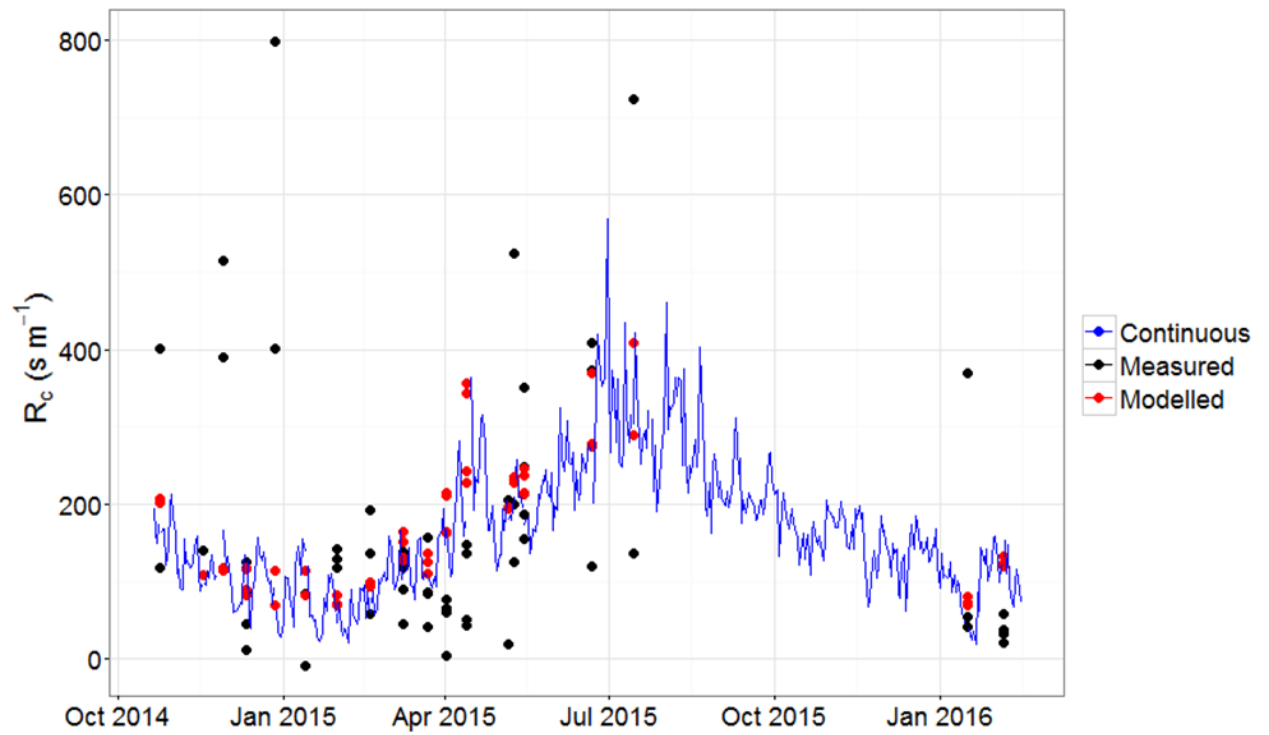
808 **Figure 2: Timeseries of time-integrated COTAG R_c measurements and Equation 4 R_c estimates. The blue line**
809 **represents continuous R_c estimates calculated from the daily mean T and RH measurements at the field site. Black**
810 **points are the measured R_c values from the COTAG systems, and the red points are the modelled R_c from the same**
811 **time-integrated data.**

812

813
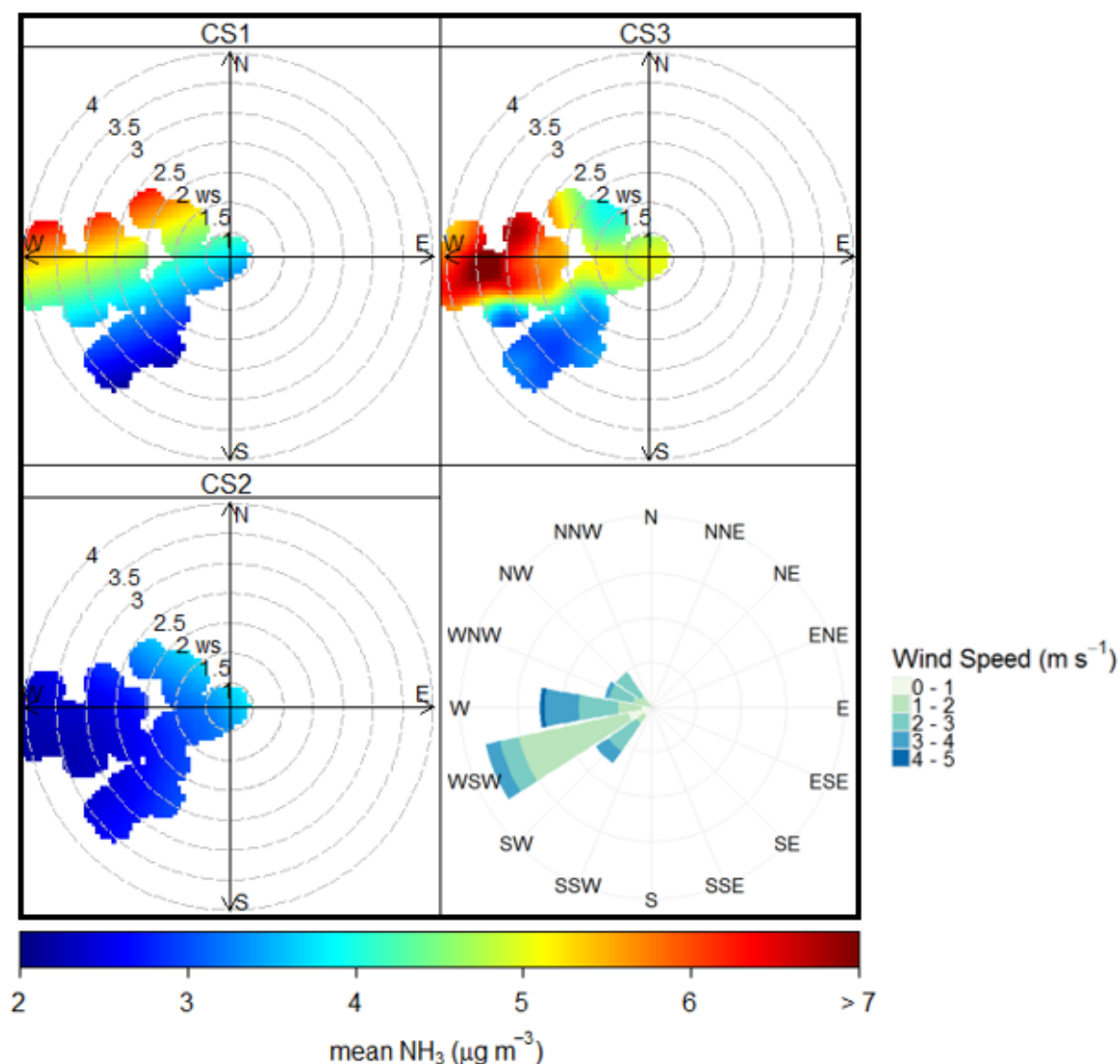
Figure 3: Polar plots showing averaged NH$_3$ concentrations (colour axis) as a function of wind speed (radial axis) and wind direction (cardinal direction) for each miniDOAS system, and a windrose showing the prevailing wind direction, Period 1 (18-20/05). The concentration Polar plots were produced using the OpenAir R package (Carslaw et al., 2014).

818

819

820

821

822

823

824

825

826

827

828
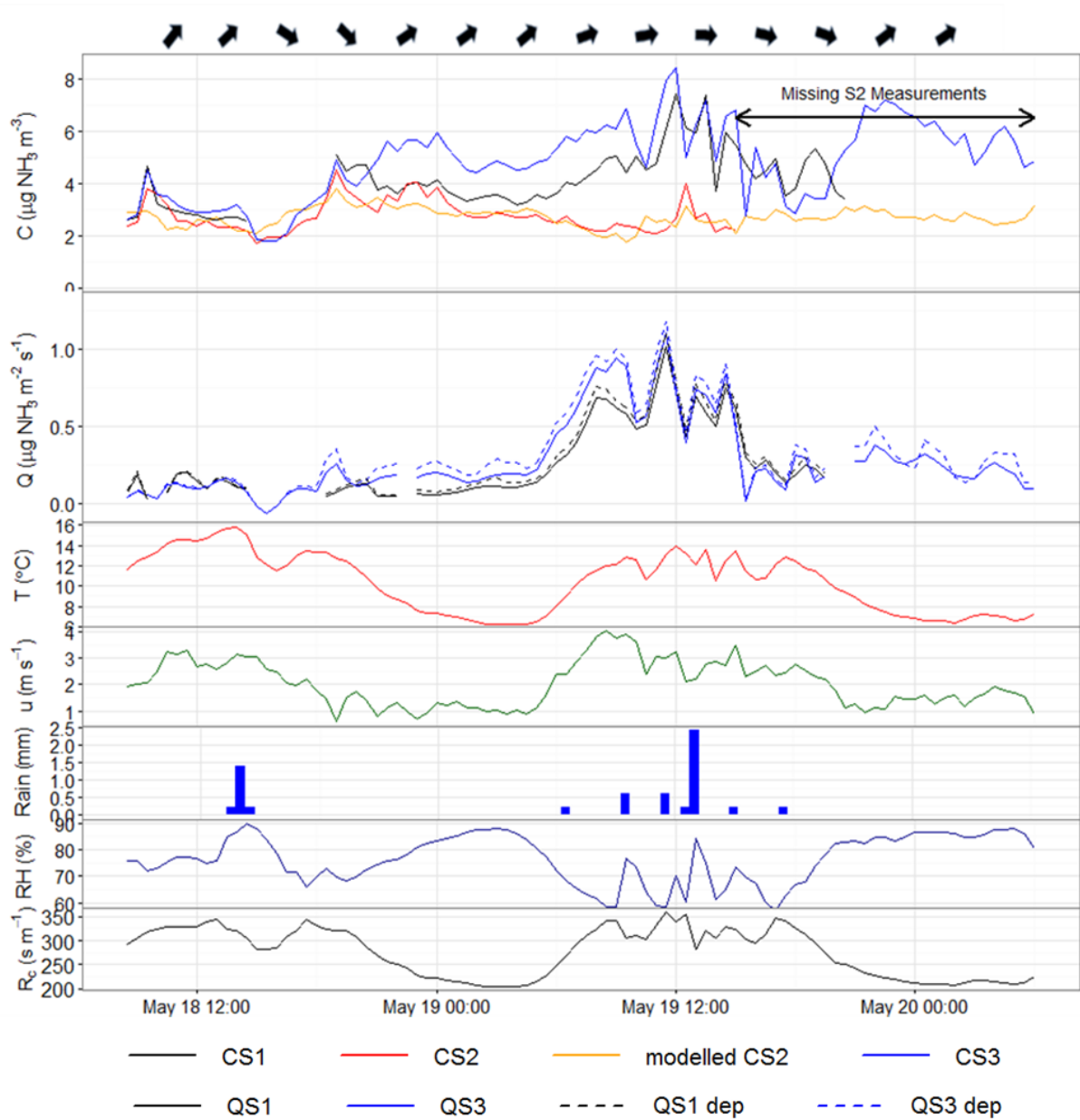
829 **Figure 4: Timeseries of Period 1 DOAS concentration measurements (CS1, CS2, CS3, and modelled CS2 using**
830 **Equation 6, top panel) and bLS-R emission estimates (Q and Q_{dep} scenarios, second panel), with T, u, Rain, RH, and**
831 **modelled R_c using Equation 5 shown in the panels below. Wind direction arrows are set above the top panel to**
832 **visualise changes over time. The cattle were present on the field for the full time period shown (08:00 18/05 - 15:00**
833 **20/05).**

834
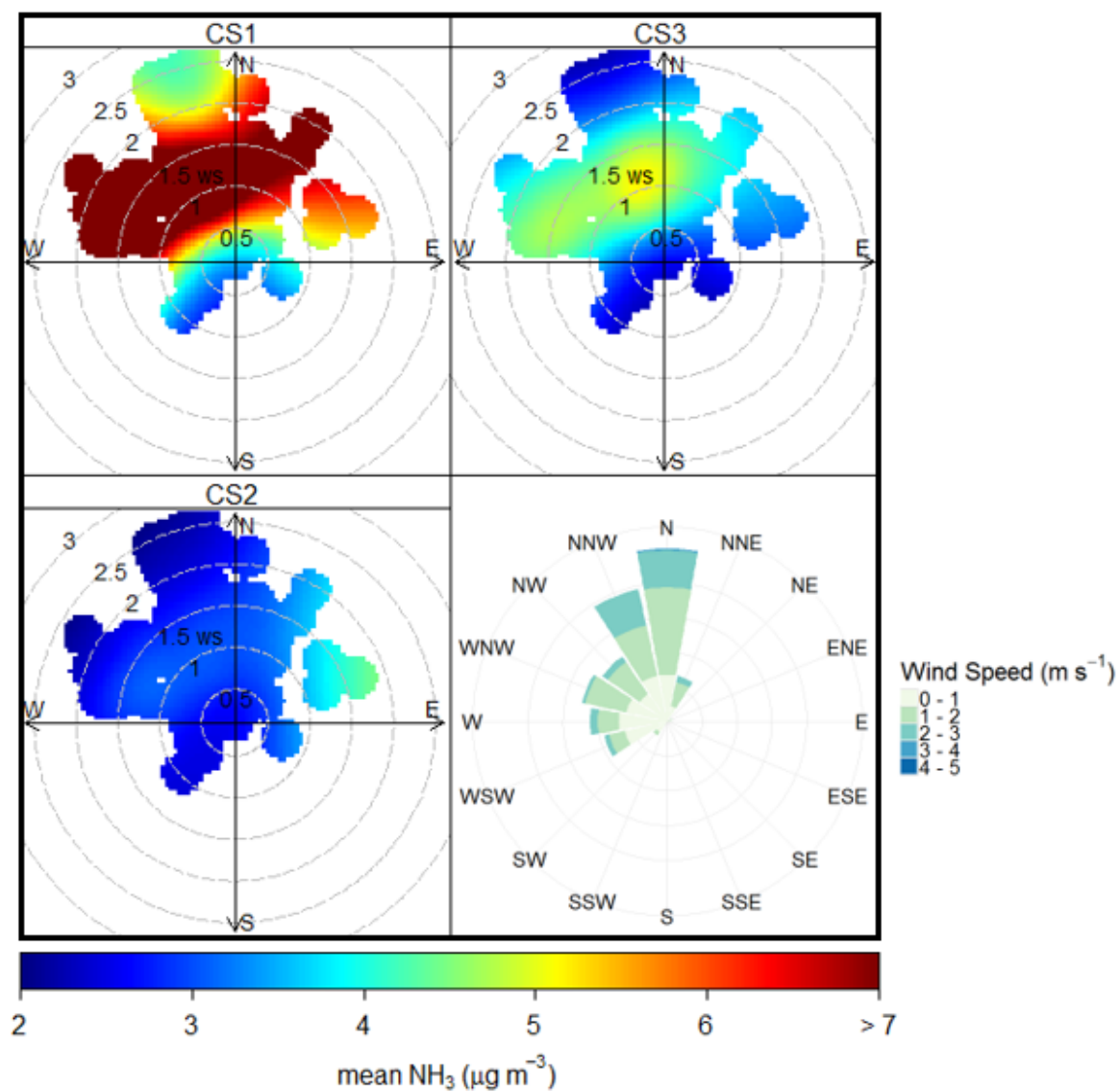
Figure 5: Polar plots showing averaged NH₃ concentrations with wind speed and direction for each DOAS system, with a windrose showing the prevailing wind directions, Period 2 (20-29/05).

837
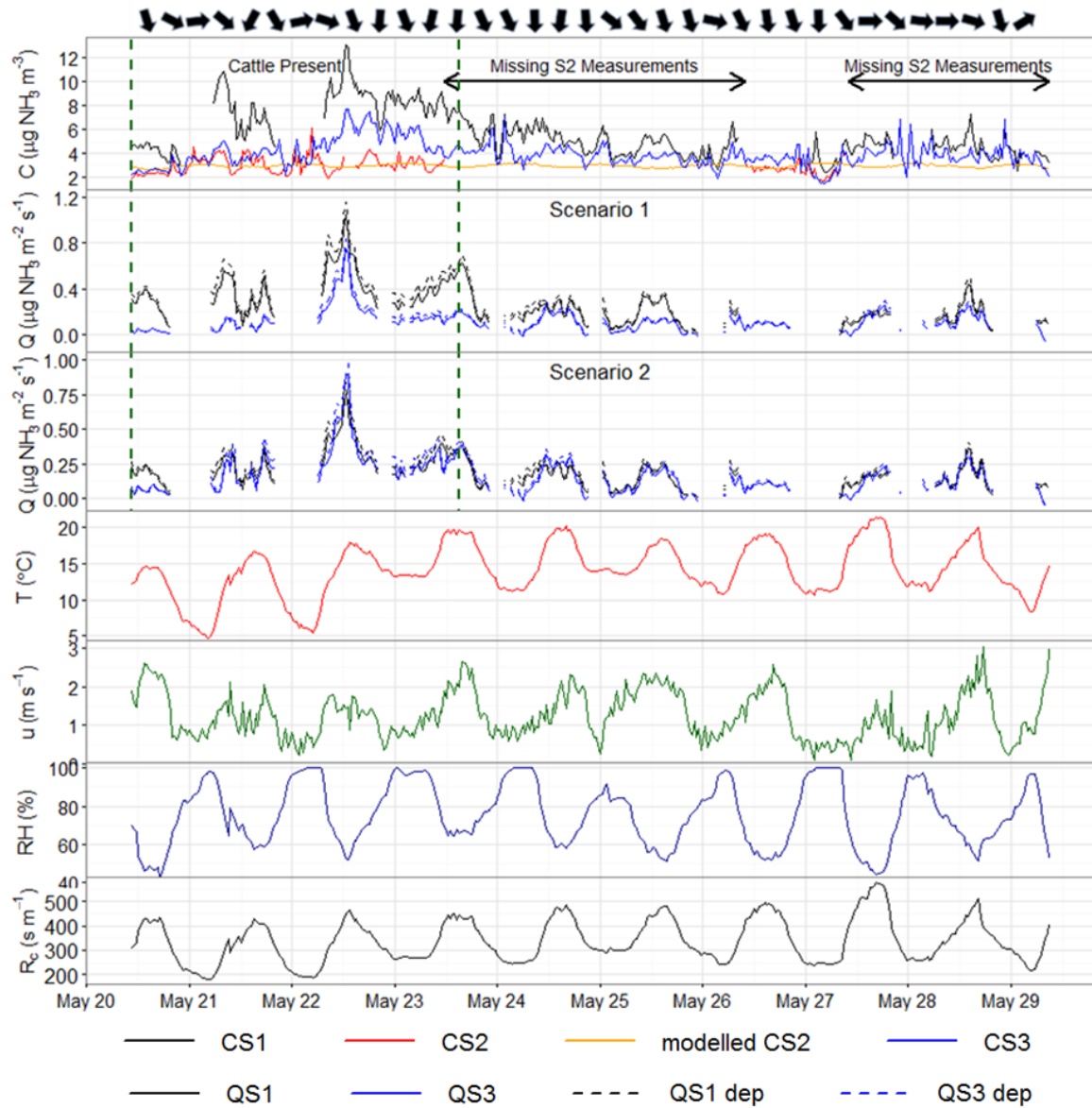
Figure 6: Timeseries of Period 2 DOAS concentration measurements (top panel) and bLS-R emission estimates (second and third panels, showing the Q (solid lines) and Q_{dep} (dashed lines) scenarios); with T, u, RH, and R_c (with 130 s m^{-1} offset) shown in the panels below. The second panel shows the Scenario 1 (homogenous field) emission estimates, while the third panel contains the optimised Scenario 2 estimates using the heterogeneous source area coefficients given in Table 1. Periods with missing S2 background concentration measurements are annotated on the top panel to highlight the higher uncertainty of these periods for emission estimates. Wind direction arrows are set above the top panel to visualise changes over time. The dashed green lines on the top panels mark the 3-day time period where the cattle were grazing the field.

846